CAMBRIDGE
UNIVERSITY PRESS

## Article

# Efficient removal of crystal violet from solution by montmorillonite modified with docosyl-trimethylammonium chloride and sodium dodecyl sulfate: modelling, kinetics and equilibrium studies

Malihe Sarabadan[1], Hadis Bashiri[1]* and Seyed Mahdi Mousavi[2]

[1]Department of Physical Chemistry, Faculty of Chemistry, University of Kashan, Kashan, Iran and [2]Department of Applied Chemistry, Faculty of Chemistry, University of Kashan, Kashan, Iran

## Abstract

Two novel modified montmorillonite (Mnt) components were prepared using Mnt nanoparticles and two surfactants: docosyl-trimethylammonium chloride (BTAC) and sodium dodecyl sulfate (SDS). These modified Mnts were used to remove a carcinogenic and harmful dye, crystal violet (CV), from solution. Optimization and modelling studies of the adsorption of these two modified Mnts were performed using response surface methodology. Four influential variables (concentration of adsorbent, temperature, pH and CV concentration) were studied to obtain the optimum conditions for CV removal. The optimal values of these variables for the two modified Mnts yielded 100% dye-removal efficiency. The optimum conditions for CV adsorption on Mnt-BTAC and Mnt-BTAC-SDS, respectively, are temperatures of 25.00 and 33.29°C, pH values of 9 and 10.1, CV concentrations of 50.00 and 10.44 mg L$^{-1}$ and adsorbent concentrations of 1.00 and 0.98 g L$^{-1}$. In equilibrium studies of the two modified Mnts, the Temkin isotherm was selected as an appropriate model, and in kinetic studies of these Mnts, the fractal-like integrated kinetics Langmuir model was found to be the best model. The Mnt-BTAC-SDS component is an affordable adsorbent with high adsorption capacity for CV.

Dyes have broad uses in various industries, but their release into aqueous systems causes environmental problems. Some dyes are toxic and hazardous to public health. Crystal violet (CV) is a toxic and carcinogenic cationic dye (Yang *et al.*, 2014; Sarabadan *et al.*, 2019b; Falaki & Bashiri, 2021; Sarabadan *et al.*, 2021). CV has several applications in the textile, paper, medicine and plastic industries (Li, 2010).

For the purification of water, several methods have been employed and amongst them adsorption is the most used technique (Eris & Bashiri, 2016; Bashiri & Nesari, 2019; Sarabadan *et al.*, 2019a; Falaki & Bashiri, 2021; Sarabadan *et al.*, 2021). Response surface methodology (RSM) is an operational approach to investigating the variables that affect the purification of water *via* absorption. It helps us to design the experiments and obtain the optimum conditions for use over the least possible time (Mousavi *et al.*, 2014; Mousavi & Nakhostin Panahi, 2016). We have used RSM previously to optimize CV dye adsorption on zeolite (Sarabadan *et al.*, 2019b), zeolite–montmorillonite (Sarabadan *et al.*, 2019a), montmorillonite–hyamine (Sarabadan *et al.*, 2021) and montmorillonite–hyamine–sodium dodecyl sulfate (SDS) (Sarabadan *et al.*, 2021) adsorbents.

Clay minerals are suitable adsorbents for wastewater treatment because they are non-toxic, inexpensive, available widely and have a large specific surface area (Ali *et al.*, 2012; Chen *et al.*, 2016). Montmorillonite (Mnt; Warr, 2020) is a layer silicate that is suitable for the adsorption of dyes, especially cationic dyes (Zhu *et al.*, 2014; Sarma *et al.*, 2016). However, untreated Mnt cannot be applied as an effective adsorbent. Previous work has investigated the adsorption capacity of clay minerals with various additives and has indicated that the adsorption of pollutants on clay minerals increases when the interlayer cations are replaced by organic cations (Carrizosa *et al.*, 2001; Koh & Dixon, 2001; Andrades *et al.*, 2004). The Mnt layers possess a negative charge and are hydrated strongly. Cationic surfactants render the hydrophilic surface of Mnt as hydrophobic (Shirzad-Siboni *et al.*, 2015). Liu *et al.* (2011) modified Mnt using surfactants and microwave irradiation for the removal of methyl orange. Acisli *et al.* (2016) used Mnt modified with dodecyltrimethylammonium bromide (DTMA) to remove acid red 17 from aqueous solution, and Kıranşan *et al.* (2014) investigated the removal efficiency of Mnt–cetyltrimethylammonium bromide (CTAB) for acid orange. Surfactants have various types of chains and head groups. Recently, we utilized the hyamine surfactant to modify Mnt nanoparticles for efficient dye removal from aqueous solution (Sarabadan *et al.*, 2021). Although Mnt is a low-cost material, the presence of hyamine as an expensive surfactant renders the cost of the combined adsorbent expensive. Therefore, we decided to synthesize an adsorbent using a lower-cost surfactant. The docosyl-trimethylammonium chloride (BTAC) surfactant is

cheaper than hyamine. It is a cationic surfactant with significant water solubility, non-toxicity and biodegradability.

Mnt nanoparticles have a small particle size. Although they have large specific surface area that improves their adsorption capacity, separation of the adsorbent from the whole solution is a complex process. Mnt nanoparticles cannot be separated by centrifugation at 9000 rpm from a solution. In this study, we prepared Mnt-BTAC and Mnt-BTAC-SDS to overcome these separation difficulties during CV adsorption, and the adsorption performances of two Mnts modified by BTAC and SDS were compared. In addition, the essential variables for CV removal were studied using RSM, and kinetic, equilibrium, thermodynamic and optimization studies of CV adsorption on the two surfactant-modified Mnt components were performed.

## Experimental

### Materials

The Mnt was purchased from Southern Clay Products, Inc. (Tx, USA). The specific gravity of Mnt nanoparticles is $0.7 \text{ g cm}^{-3}$. Mnt has a cation-exchange capacity of 48 meq $100 \text{ g}^{-1}$ and particle sizes of 1 nm–2 μm. The chemical composition of Mnt is 50.95% $SiO_2$, 19.60% $Al_2O_3$, 5.62% $Fe_2O_3$, 3.29% MgO, 1.97% CaO, 0.98% $Na_2O$, 0.86% $K_2O$, 0.62% $TiO_2$ and 15.45% loss on ignition. BTAC ($CH_3(CH_2)_{21}N(Cl)(CH_3)_3$) with 98% purity and SDS ($NaC_{12}H_{25}SO_4$) with 85% purity were purchased from Merck Co. (Germany). Figure 1 shows the molecular structures of the BTAC and SDS surfactants. CV ($C_{25}H_{30}N_3Cl$) was procured from Merck; 1.00 g CV powder was dissolved in 1000 mL of deionized water.

### Characterization of the surfactants

The structure of the surfactant-modified Mnt was studied using X-ray diffraction (XRD) with Cu-*K*α radiation (Philips X'Pert Pro MPD diffractometer). The specific surface area of the surfactant-modified Mnt was determined using a BET Sorb Gas Adsorption Analyzer (BEL Company, Japan). Fourier-transform infrared (FTIR) absorption spectra of the surfactant-modified Mnt were collected using a Nicolet Magna 550 FTIR spectrometer. The morphology of the materials was studied using field-emission scanning electron microscopy (FE-SEM) with a TESCAN MIRA3 FE-SEM. The absorbance spectra of the materials were obtained using ultraviolet–visible light (UV–Vis) spectrophotometry with a Shimadzu model T-80 UV–Vis spectrophotometer.

### Preparation of the Mnt-BTAC and Mnt-BTAC-SDS components

The purified Mnt was obtained by dispersing Mnt nanoparticles in deionized water (20 g in 400 mL) under stirring for 2 h at

1500 rpm, followed by centrifugation at 6000 rpm for 25 min and drying at 100°C for 8 h. To synthesize Mnt-BTAC component, the purified Mnt nanoparticles were dispersed in deionized water (10 g in 300 mL) and stirred for 10 h at 1000 rpm. Then, the desired amount of BTAC surfactant (20% of adsorbent weight) was slowly added and stirred at 2000 rpm for 1.5 h. Subsequently, the suspension was filtered and washed thoroughly and dried at 95°C for 12 h. To synthesize the Mnt-BTAC-SDS component, 10 g of the purified Mnt was dispersed in 300 mL of deionized water under stirring (1000 rpm) at 70°C for 1.5 h. Then, 6 g of BTAC surfactant was slowly added under stirring (2000 rpm) at 70°C for 2 h. Subsequently, 2.4 g of SDS surfactant was added under stirring for 1.5 h. The mixture was filtered, washed thoroughly and dried at 95°C for 12 h.

### Adsorption experiments

For the equilibrium study of CV removal by Mnt-BTAC, 50 mL of dye solution at concentrations of $10–90 \text{ mg L}^{-1}$ were added to 50 mL of Mnt-BTAC and stirred in a shaker at 130 rpm for 24 h. For the equilibrium study of CV removal by Mnt-BTAC-SDS, 50 mL of dye solution at concentrations of $10–100 \text{ mg L}^{-1}$ and $0.98 \text{ g L}^{-1}$ of Mnt-BTAC-SDS were stirred in a shaker at 130 rpm for 24 h. For the study of the adsorption kinetics, $1.00 \text{ g L}^{-1}$ of Mnt-BTAC or $0.98 \text{ g L}^{-1}$ of Mnt-BTAC-SDS were added to 50 mL of CV solution at concentrations of 4, 6, 8 or $10 \text{ mg L}^{-1}$. The solutions were placed in a shaker and stirred at 130 rpm for 300 min. For a detailed description of the equilibrium and kinetics studies, see our previous study (Sarabadan *et al.*, 2019a).

### Experimental design

To determine the importance of various variables on CV removal efficiency, we used the central composite design (CCD) method. Four variables were examined: pH (*A*), temperature (*B*), concentration of adsorbent (*C*) and CV concentration (*D*). Their actual values are presented in Table 1. For the two Mnts modified by BTAC and SDS, 30 experimental runs were performed. The dye-removal efficiencies achieved for the Mnt-BTAC and Mnt-BTAC-SDS components were 92.50–99.95% and 81.00–99.47%, respectively (Table 2). The relationship between the response and the variables is given in Equation 1:

$$y = \beta_0 + \sum_{i=1}^{4} \beta_i x_i + \sum_{i=1}^{4} \beta_{ii} x_i^2 + \sum_{i=1}^{4} \sum_{j=1}^{4} \beta_{ij} x_i x_j + \varepsilon \qquad (1)$$

where *y* is the response, $\beta_0$, $\beta_i$, $\beta_{ii}$ and $\beta_{ij}$ are a constant, the linear effect term, the quadratic effect and the interaction effect term,
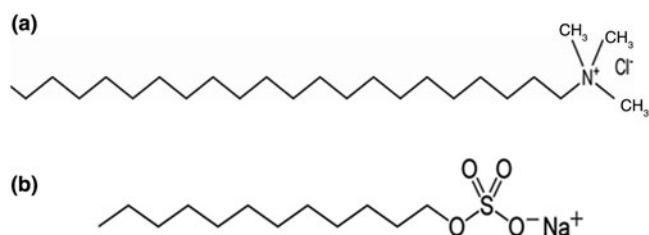


**Fig. 1.** The chemical structures of the (a) BTAC and (b) SDS surfactants.

**Table 1.** The experimental levels of the variables for the Mnts modified with BTAC and SDS.

| Independent variables | Levels | | | | |
|---|---|---|---|---|---|
| | −2 (−α) | −1 | 0 | 1 | +2 (+α) |
| pH (*A*) | 3 | 5 | 7 | 9 | 11 |
| Temperature (°C, *B*) | 25.0 | 32.5 | 40.0 | 47.5 | 55.0 |
| Concentration of adsorbent (g $L^{-1}$, *C*) | 0.5 | 1.0 | 1.5 | 2.0 | 2.5 |
| CV concentration (mg $L^{-1}$, *D*) | 10.0 | 32.5 | 55.0 | 77.5 | 100 |

**Table 2.** CCD matrix and the response values for the Mnts modified with BTAC and SDS.

| Run | pH | Temperature (°C) | Concentration of adsorbent (g L$^{-1}$) | CV concentration (mg L$^{-1}$) | Removal efficiency (%) with Mnt-BTAC | Removal efficiency (%) with Mnt-BTAC-SDS |
|---|---|---|---|---|---|---|
| 1 | 7 | 40.0 | 1.5 | 55.0 | 99.61 | 84.80 |
| 2 | 9 | 47.5 | 2.0 | 77.5 | 99.54 | 95.50 |
| 3 | 7 | 40.0 | 1.5 | 55.0 | 99.00 | 84.90 |
| 4 | 7 | 25.0 | 1.5 | 55.0 | 98.82 | 81.00 |
| 5 | 9 | 32.5 | 2.0 | 77.5 | 99.13 | 89.80 |
| 6 | 5 | 47.5 | 2.0 | 77.5 | 98.35 | 90.00 |
| 7 | 9 | 55.0 | 1.5 | 55.0 | 99.84 | 88.00 |
| 8 | 7 | 40.0 | 1.5 | 55.0 | 98.00 | 84.70 |
| 9 | 9 | 32.5 | 1.0 | 77.5 | 97.12 | 88.00 |
| 10 | 9 | 32.5 | 2.0 | 32.5 | 99.12 | 95.00 |
| 11 | 7 | 40.0 | 1.5 | 10.0 | 99.83 | 94.00 |
| 12 | 9 | 47.5 | 1.0 | 77.5 | 99.22 | 88.60 |
| 13 | 5 | 32.5 | 1.0 | 32.5 | 93.81 | 88.00 |
| 14 | 7 | 40.0 | 1.5 | 100 | 98.22 | 91.20 |
| 15 | 7 | 40.0 | 0.5 | 55.0 | 94.65 | 83.50 |
| 16 | 9 | 32.5 | 1.0 | 32.5 | 98.46 | 90.00 |
| 17 | 5 | 32.5 | 2.0 | 32.5 | 97.38 | 88.00 |
| 18 | 7 | 40.0 | 1.5 | 55.0 | 98.90 | 82.90 |
| 19 | 3 | 40.0 | 1.5 | 55.0 | 92.50 | 85.00 |
| 20 | 5 | 32.5 | 1.0 | 77.5 | 94.80 | 85.00 |
| 21 | 5 | 47.5 | 1.0 | 32.5 | 96.65 | 88.00 |
| 22 | 7 | 40.0 | 1.5 | 55.0 | 99.50 | 84.70 |
| 23 | 7 | 40.0 | 2.5 | 55.0 | 99.95 | 91.81 |
| 24 | 7 | 40.0 | 1.5 | 55.0 | 99.10 | 85.30 |
| 25 | 5 | 32.5 | 2.0 | 77.5 | 97.45 | 87.00 |
| 26 | 5 | 47.5 | 1.0 | 77.5 | 94.12 | 84.00 |
| 27 | 5 | 47.5 | 2.0 | 32.5 | 98.31 | 92.00 |
| 28 | 9 | 47.5 | 1.0 | 32.5 | 99.57 | 96.00 |
| 29 | 11 | 40.0 | 1.5 | 55.0 | 99.79 | 99.47 |
| 30 | 7 | 55.0 | 1.5 | 55.0 | 99.58 | 88.00 |

respectively, $x_i$ and $x_j$ are variables and $\varepsilon$ is the residual of the model.

## Results and discussion

### Characteristics of the surfactant-modified Mnts

The FTIR spectra of Mnt nanoparticles (Sarabadan *et al.*, 2021), Mnt-BTAC and Mnt-BTAC-SDS are presented in Fig. 2. For Mnt nanoparticles, a broad band at ~3429 cm$^{-1}$ is attributed to stretching vibrations of H$_2$O. The band at 1635 cm$^{-1}$ in Mnt-BTAC is due to H–O–H bending. In the case of Mnt nanoparticles, the band at 900–1100 cm$^{-1}$ is attributed to Si–O stretching (Santhana Krishna Kumar *et al.*, 2012). In Mnt-BTAC, the bands at 2921 and 2850 cm$^{-1}$ are assigned to C–H stretching. The lack of these bands in the spectrum of Mnt nanoparticles and the sharp band at 1471 cm$^{-1}$ in the Mnt-BTAC spectrum indicate the existence of BTAC molecules in the Mnt-BTAC component. In Mnt-BTAC-SDS, the increased intensities of the bands at 2921 and 2850 cm$^{-1}$ are attributed to C–H stretching in the BTAC and SDS molecules having increased.

The XRD traces of Mnt nanoparticles (Sarabadan *et al.*, 2021), Mnt-BTAC and Mnt-BTAC-SDS are shown in Fig. 3. By adding BTAC and SDS surfactants, the intensities of the main reflections decrease. In addition, the reflection at 7°2θ in Mnt nanoparticles is not present in the traces of Mnt modified with BTAC and SDS because Na$^+$ ions in Mnt nanoparticles are replaced by BTAC molecules (Shirzad-Siboni *et al.*, 2015). The reflections in the XRD traces of Mnt nanoparticles and surfactant-modified Mnt at 22.5°2θ are attributed to gypsum and the reflections at 27.5°2θ are due to quartz.

The N$_2$ adsorption–desorption analysis results for the Mnts modified by BTAC and SDS are presented in Table 3. For Mnt-BTAC, the Brunauer–Emmett–Teller (BET) surface area and total pore volume are 7 m$^2$ g$^{-1}$ and 0.058 cm$^3$ g$^{-1}$, respectively, and the mean pore diameter is 34.9 nm. For Mnt-BTAC-SDS, the BET surface area and total pore volume are 4 m$^2$ g$^{-1}$ and 0.024 cm$^3$ g$^{-1}$, respectively, and the mean pore diameter is 22.5 nm. The N$_2$ adsorption–desorption isotherms of the two modified Mnt components are classified as type V according to the International Union of Pure and Applied Chemistry (IUPAC) classification system (Fig. 4). Therefore, these are mesoporous materials with not well-defined pore shapes (Park *et al.*, 2013). Mnt-BTAC has a larger specific surface area than Mnt-BTAC-SDS, while Mnt-BTAC-SDS has a larger adsorption capacity than Mnt-BTAC. The anionic SDS molecules interact with cationic CV molecules, thereby contributing to dye adsorption on Mnt-BTAC-SDS.

The surface morphology and particle sizes of the two modified Mnts were studied using FE-SEM. FE-SEM images of Mnt nanoparticles (Sarabadan *et al.*, 2021), Mnt-BTAC and Mnt-BTAC-SDS are shown in Fig. 5. The Mnt nanoparticle sheets are thicker than those of Mnt-BTAC and Mnt-BTAC-SDS. After modification, the Mnt structure changes to an irregular-layered structure, indicating an increase of the Mnt surface area due to the modification. The thickness of Mnt particles is ~5–10 nm (Fig. 5a)

Energy-dispersive X-ray analysis (EDX) spectra of Mnt modified with BTAC and SDS are shown in Fig. 6. For Mnt-BTAC, the weight percentages of C, O, Si, Fe, Al, K, Ca, Mg and Ti are 27.2, 42.3, 17.8, 3.4, 7.8, 0.48, 0.26, 0.35 and 0.21 wt.%, respectively, while Na is absent. For Mnt-BTAC-SDS, the weight percentages of O, C, Si, S, Al, Fe, Mg, K, Ti, Ca and Na are 32.3, 43.2, 12.8, 1.97, 5.9, 1.8, 0.58, 0.64, 0.22, 0.30 and 0.17 wt.%, respectively.
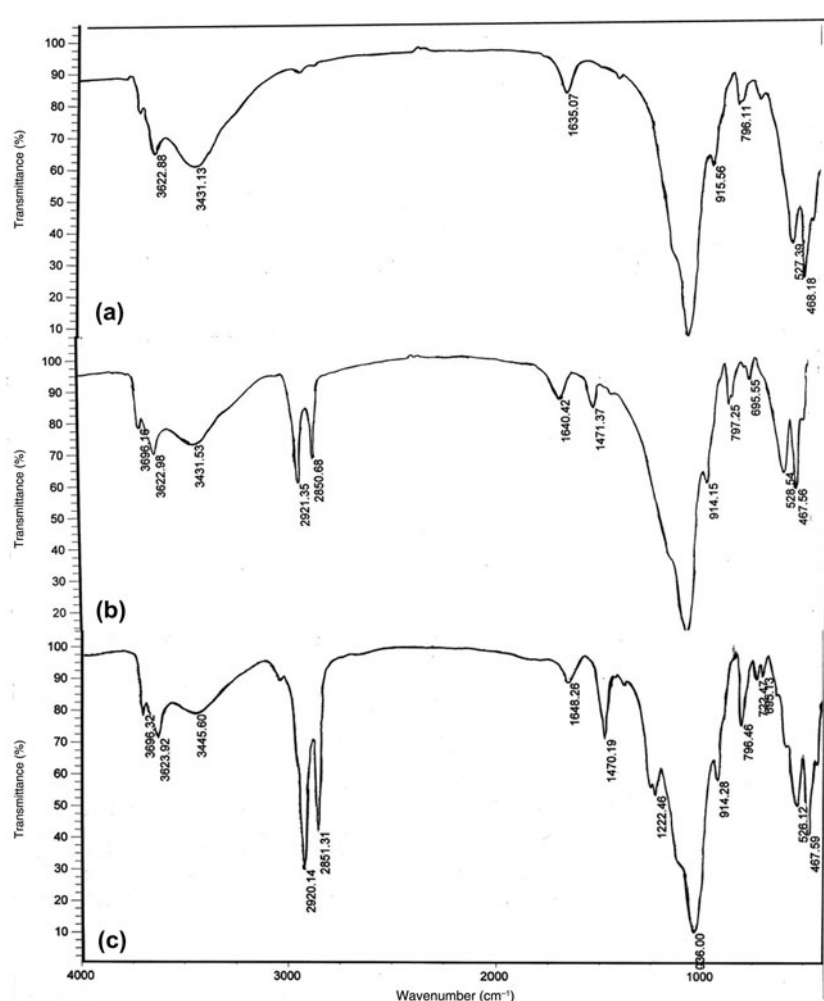
**Fig. 2.** FTIR spectra of (a) Mnt nanoparticles, (b) Mnt-BTAC and (c) Mnt-BTAC-SDS.

The Na concentration in Mnt nanoparticles is 0.80 wt.%, which decreases in Mnt-BTAC and Mnt-BTAC-SDS. The Na$^+$ ions in the Mnt layers are replaced by the surfactants through their addition to the Mnt nanoparticles. BTAC is a cationic surfactant and so it can be replaced by Na$^+$ ions in the Mnt layers *via* cation exchange.

## RSM analysis

*Regression model equation and statistical analysis.* A quadratic model was generated to demonstrate the correlations between the four variables and the response. The equations obtained for the Mnts modified with BTAC and SDS are given in Equations 2 and 3:

$$R_{Mnt-BTAC} = 99.02 + 1.49A + 0.41B + 1.08C - 0.28D$$
$$+ 0.022AB - 0.55AC - 0.034AD - 0.15BC - 0.18BD$$
$$+ 0.19CD - 0.76A^2$$
$$+ 0.005729B^2 - 0.47C^2 - 0.038D^2$$

$$(2)$$

$$R_{Mnt-BTAC-SDS} = 84.40 + 2.49A + 1.14B + 2.01C - 1.03D$$
$$+ 0.081AB + 0.48AC + 0.056AD$$
$$+ 0.88BC + 0.21BD + 0.11CD + 2.03A^2$$
$$+ 0.097B^2 + 0.89C^2 + 2.12D^2$$

$$(3)$$

These equations for the Mnts modified with BTAC and SDS show that the variables A, B and C have positive effects on the response, with pH (A) having the greatest contribution. The D variable has a negative effect on the response.

*ANOVA results.* The results of the analysis of variance are presented in Tables 4 & 5. A P-value > 0.1 suggests that the terms of the model are not significant, whereas a P-value < 0.0001 indicates that the model terms are highly significant. For CV adsorption on Mnt modified with BTAC and SDS, the F-values are 15.61 and 16.89, respectively, and the P-values are <0.0001 (Tables 4 & 5), implying that the model used to design the experiments is significant. For Mnt-BTAC, the A, B, C, AC, $A^2$ and $C^2$ model terms are significant, while for Mnt-BTAC-SDS, the A, C, D, BC, $A^2$, $C^2$ and $D^2$ model terms are significant. The low coefficient of variation values (0.74% for Mnt-BTAC and 1.70% for Mnt-BTAC-SDS) indicate that the experiments are accurate. The predicted $R^2$ values for Mnt-BTAC (0.6883) and Mnt-BTAC-SDS (0.6861) are in reasonable agreement with the adjusted $R^2$ values of 0.8759 and 0.8847, respectively. In addition, the $R^2$ values obtained for Mnt modified with BTAC and SDS are 0.9358 and 0.9404, respectively.

The percentage effect of each variable on dye-removal efficiency was investigated using Pareto analysis. The Pareto analyses for Mnt-BTAC and Mnt-BTAC-SDS show that pH is the variable that has the greatest impact on CV removal (Fig. 7). The actual values obtained from a specific run and the predicted values
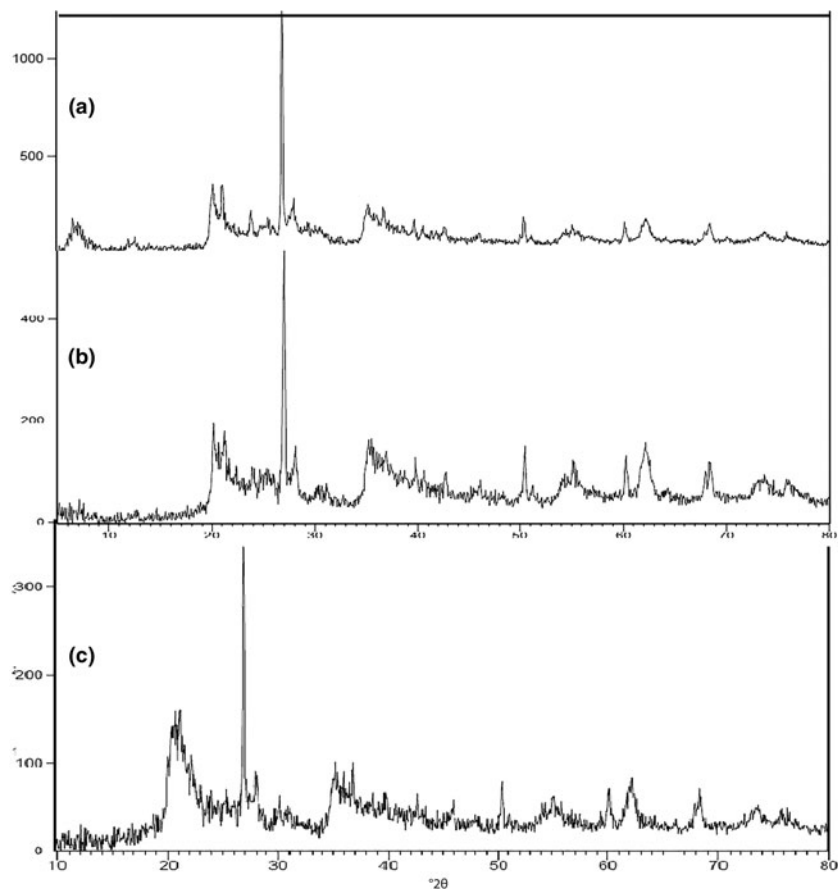
**Fig. 3.** XRD traces of (a) Mnt nanoparticles, (b) Mnt-BTAC and (c) Mnt-BTAC-SDS.

calculated from the models of the Mnts modified with BTAC and SDS are distributed along a reasonably straight line (Fig. 8), indicating good agreement between the predicted and observed values.

### CCD plots

The perturbation plots from the selected models for Mnt-BTAC and Mnt-BTAC-SDS also show that pH is the variable that has the greatest impact on CV removal. In addition, the concentration of adsorbent, temperature and pH have positive effects on CV removal. In contrast, the CV concentration has a negative influence on CV removal (Fig. 9).

The CCD plots indicate the importance of the various variables for the response of CV removal (Agarwal *et al.*, 2016). Figure 10 shows the response surface plots for Mnt-BTAC and Mnt-BTAC-SDS. The pH, temperature, concentration of adsorbent and CV concentration are marked as *A*, *B*, *C* and *D*, respectively. Dye adsorption increases with pH and temperature (Fig. 10a,d).

With increasing pH and temperature, the number of negative sites for adsorbents increases, thereby increasing the adsorption of the cationic CV dye. The plot of the interactive effect of pH and concentration of adsorbent (Fig. 10b,e) shows that dye removal increases with concentration of adsorbent because of the large

**Table 3.** The specific surface area and total pore volume of the Mnts modified with BTAC and SDS.

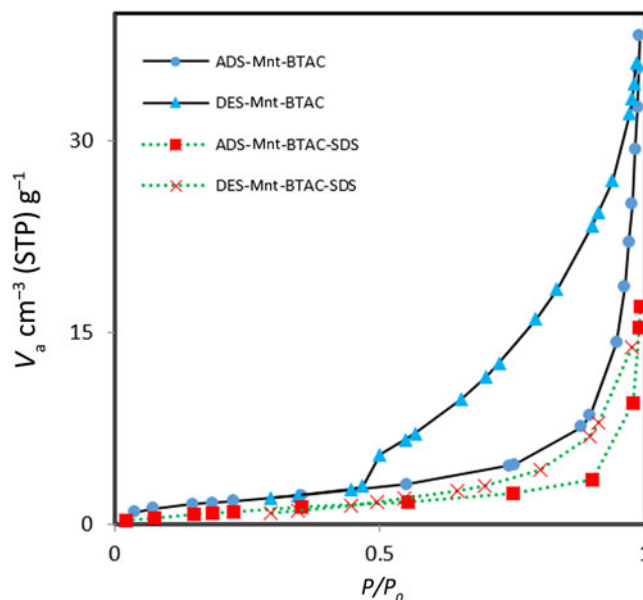| Parameter | Mnt-BTAC | Mnt-BTAC-SDS |
|---|---|---|
| Barrett–Joyner–Halenda cumulative surface area ($m^2\ g^{-1}$) | 9 | 5 |
| Mean pore diameter (nm) | 34.9 | 22.5 |
| BET surface area ($m^2\ g^{-1}$) | 7 | 4 |
| Total pore volume ($cm^3\ g^{-1}$) | 0.058 | 0.024 |



**Fig. 4.** $N_2$ adsorption–desorption isotherms of Mnt-BTAC and Mnt-BTAC-SDS. STP = standard temperature and pressure. ADS = adsorption; DES = desorption.
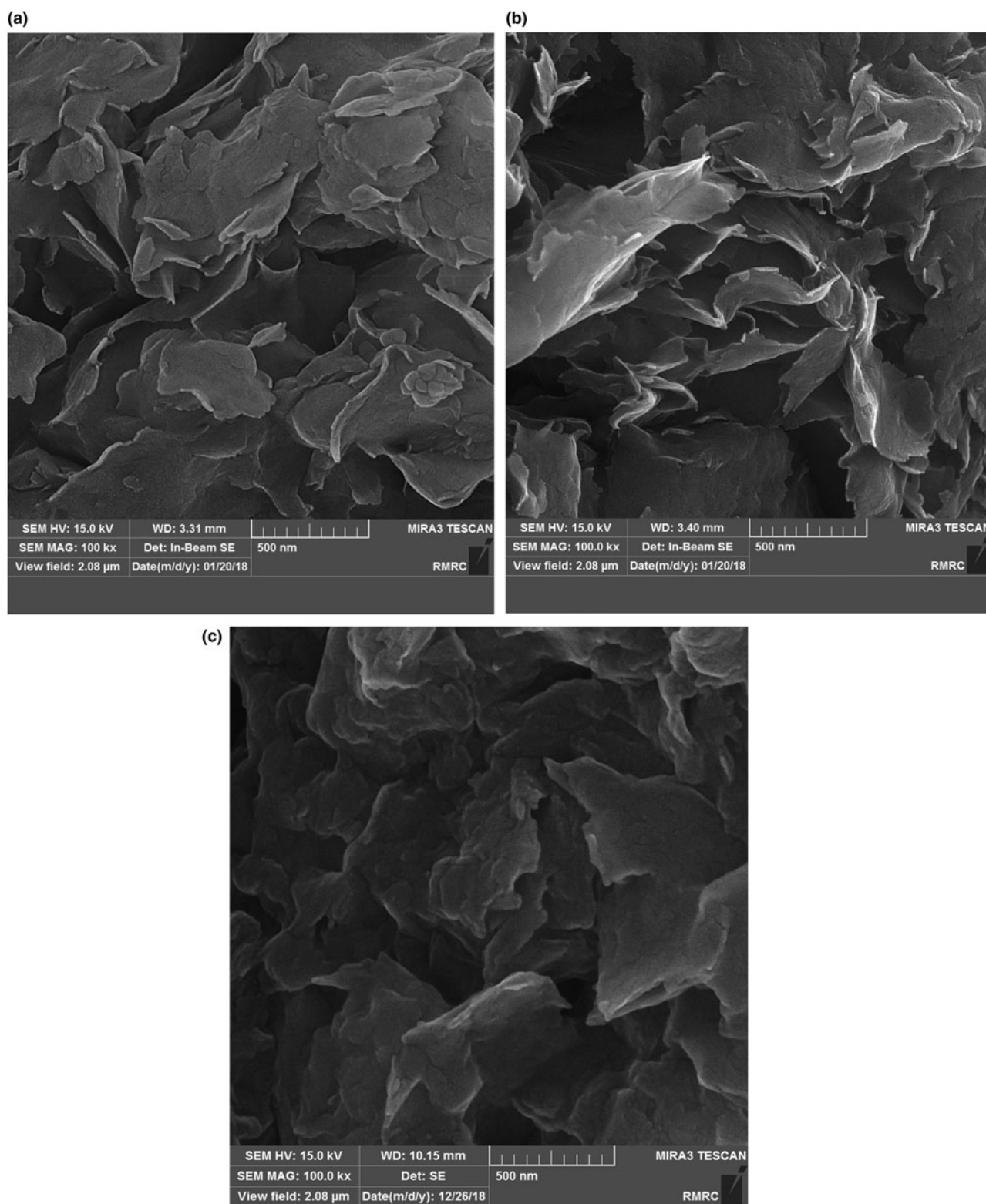
**Fig. 5.** FE-SEM images of (a) Mnt nanoparticles, (b) Mnt-BTAC and (c) Mnt-BTAC-SDS.

number of active sites. The interacting influence of pH and CV concentration shows that dye removal increases with decreasing CV concentration (Fig. 10c,f). In addition, temperature and concentration of absorbent of have positive effects on CV adsorption, whereas the CV concentration has a negative effect on dye adsorption (data not shown). When dye concentration increases at a constant concentration of adsorbent, the adsorbent sites decrease gradually, and so the dye-removal efficiency decreases. Elliptical or saddle-like contour plots demonstrate that the interaction between the variables is significant, whereas circular contour
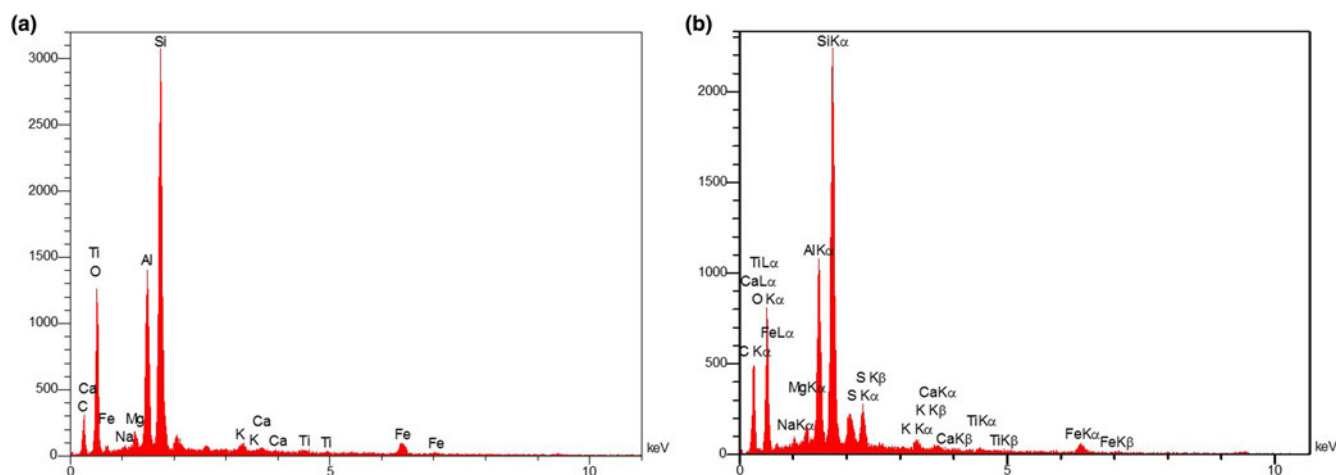
**Fig. 6.** EDX spectra of (a) Mnt-BTAC and (b) Mnt-BTAC-SDS.

plots indicate an insignificant interaction between variables. For Mnt-BTAC, the contour plots have elliptical or saddle-like shapes, and so the interactions between the various variables are significant. For Mnt-BTAC-SDS, the contour plot for the interaction of pH and dye concentration is circular, suggesting an insignificant interaction. The interactions between the remaining variables for Mnt-BTAC-SDS are significant.

### Optimization adsorption conditions

Optimization analysis was performed using *Design Expert 7.0* software to obtain the values of the influential variables that maximize the dye-removal efficiency. For Mnt-BTAC, total dye removal (100%) was observed at pH 9, concentration of adsorbent 1 g L$^{-1}$, temperature 25°C and CV concentration 50 mg L$^{-1}$. The

optimum CV concentration for the Mnt–hyamine adsorbent has been reported as 30 mg L$^{-1}$ (Sarabadan *et al.*, 2021). At optimum conditions, Mnt-BTAC was more effective for CV removal than Mnt–hyamine.

For Mnt-BTAC-SDS, total dye removal was observed at pH 10.1, temperature 33.3°C, concentration of adsorbent 0.98 g L$^{-1}$ and CV concentration 10.44 mg L$^{-1}$. Desirability values of 1.00 (indicating an ideal response) were obtained at these optimum conditions.

### Adsorption isotherms

Equilibrium studies for CV adsorption on Mnt-BTAC were performed for the solutions with CV concentrations of 10–90 mg L$^{-1}$ at the optimal values of temperature, pH and

**Table 4.** ANOVA for Mnt-BTAC.

| Source | Sum of squares | df | Mean squares | F-value | P-value |
|---|---|---|---|---|---|
| Model | 113.89 | 14 | 8.14 | 15.61 | <0.0001 |
| AA | 53.13 | 1 | 53.13 | 101.98 | <0.0001 |
| BB | 4.04 | 1 | 4.04 | 7.76 | 0.0139 |
| CC | 28.10 | 1 | 28.10 | 53.93 | <0.0001 |
| DD | 1.83 | 1 | 1.83 | 3.52 | 0.0804 |
| AB | 0.00765 | 1 | 0.00765 | 0.015 | 0.9051 |
| AC | 4.90 | 1 | 4.90 | 9.39 | 0.0079 |
| AD | 0.019 | 1 | 0.019 | 0.036 | 0.8515 |
| BC | 0.36 | 1 | 0.36 | 0.70 | 0.417 |
| BD | 0.51 | 1 | 0.51 | 0.99 | 0.3360 |
| CD | 0.58 | 1 | 0.58 | 1.12 | 0.3075 |
| $A^2$ | 15.76 | 1 | 15.76 | 30.25 | <0.0001 |
| $B^2$ | 0.0009 | 1 | 0.0009 | 0.00172 | 0.9674 |
| $C^2$ | 6.04 | 1 | 6.04 | 11.59 | 0.0039 |
| $D^2$ | 0.040 | 1 | 0.040 | 0.076 | 0.7864 |
| Residual | 7.82 | 15 | 0.52 | | |
| Lack of fit | 6.18 | 10 | 0.62 | 1.88 | 0.2514 |
| | | | | | Not significant |
| Pure error | 1.64 | 5 | 0.33 | | |
| Corrected total | 121.71 | 29 | | | |

*Model summary statistics*

| | | | |
|---|---|---|---|
| Standard deviation | 0.72 | $R^2$ | 0.9358 |
| Coefficient of variation | 0.74 | Adjusted $R^2$ | 0.8759 |
| Adequate precision | 14.393 | Predicted $R^2$ | 0.6883 |

**Table 5.** ANOVA for Mnt-BTAC-SDS.

| Source | Sum of squares | df | Mean squares | F-value | P-value |
|---|---|---|---|---|---|
| Model | 537.24 | 14 | 38.37 | 16.89 | <0.0001 |
| AA | 149.20 | 1 | 149.20 | 65.67 | <0.0001 |
| BB | 31.05 | 1 | 31.05 | 13.67 | 0.0022 |
| CC | 97.28 | 1 | 97.28 | 42.82 | <0.0001 |
| DD | 25.42 | 1 | 25.42 | 11.19 | 0.0044 |
| AB | 0.11 | 1 | 0.11 | 0.046 | 0.8322 |
| AC | 3.71 | 1 | 3.71 | 1.63 | 0.2210 |
| AD | 0.051 | 1 | 0.051 | 0.022 | 0.8833 |
| BC | 12.43 | 1 | 12.43 | 5.47 | 0.0336 |
| BD | 0.68 | 1 | 0.68 | 0.3 | 0.5922 |
| CD | 0.18 | 1 | 0.18 | 0.080 | 0.7818 |
| $A^2$ | 113.15 | 1 | 113.15 | 49.80 | <0.0001 |
| $B^2$ | 0.26 | 1 | 0.26 | 0.11 | 0.7400 |
| $C^2$ | 21.53 | 1 | 21.53 | 9.48 | 0.0076 |
| $D^2$ | 123.54 | 1 | 123.54 | 54.38 | <0.0001 |
| Residual | 34.08 | 15 | 2.27 | | |
| Lack of fit | 30.16 | 10 | 3.02 | 3.85 | 0.0750 |
| | | | | | Not significant |
| Pure error | 3.92 | 5 | 0.78 | | |
| Corrected total | 571.31 | 29 | | | |

*Model summary statistics*

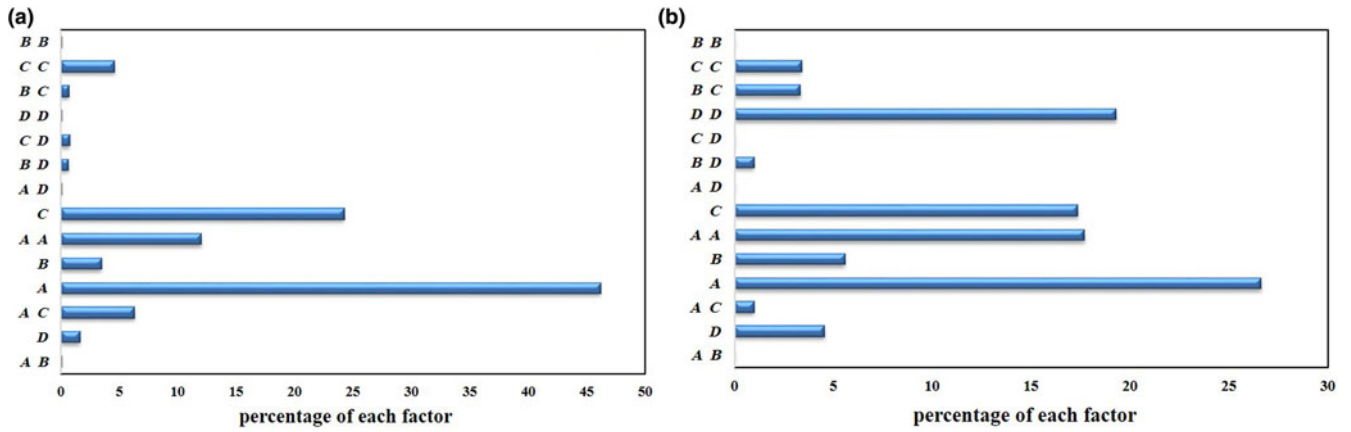| | | | |
|---|---|---|---|
| Standard deviation | 1.51 | $R^2$ | 0.9404 |
| Coefficient of variation | 1.70 | Adjusted $R^2$ | 0.8847 |
| Adequate precision | 14.071 | Predicted $R^2$ | 0.6861 |

**Fig. 7.** Pareto graphical analyses of (a) Mnt-BTAC and (b) Mnt-BTAC-SDS.
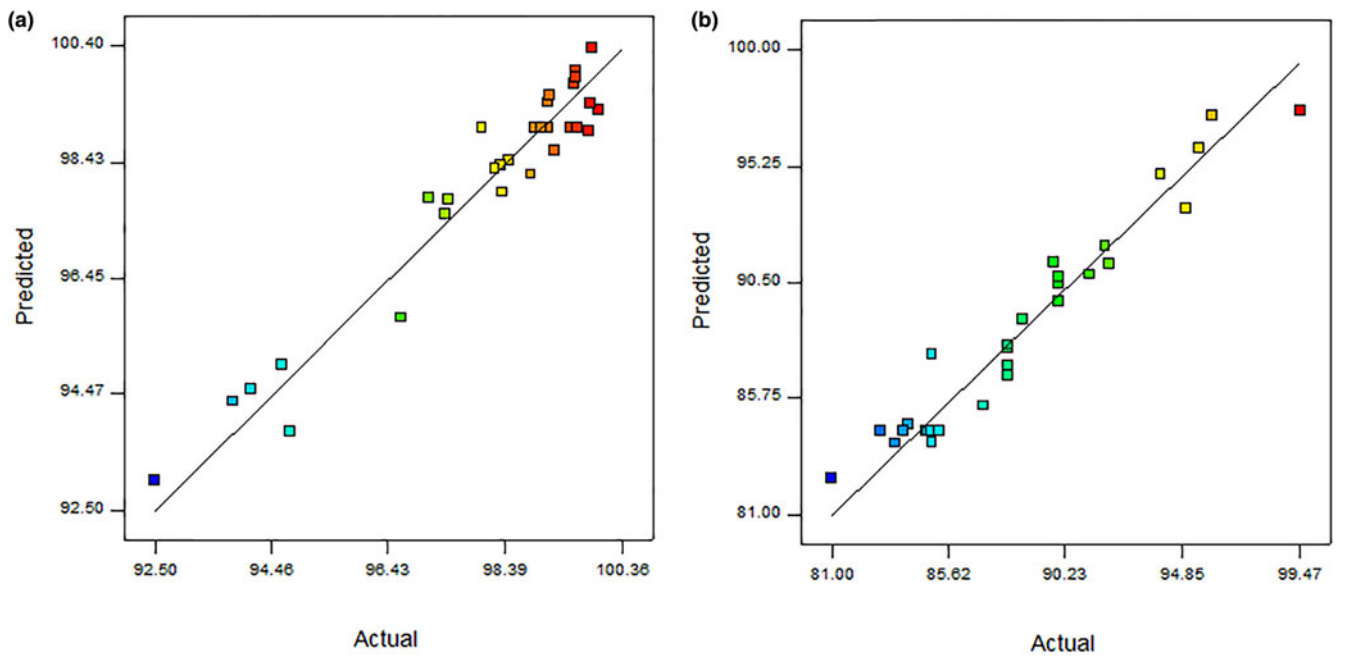


**Fig. 8.** The predicted *vs* actual data for (a) Mnt-BTAC and (b) Mnt-BTAC-SDS.
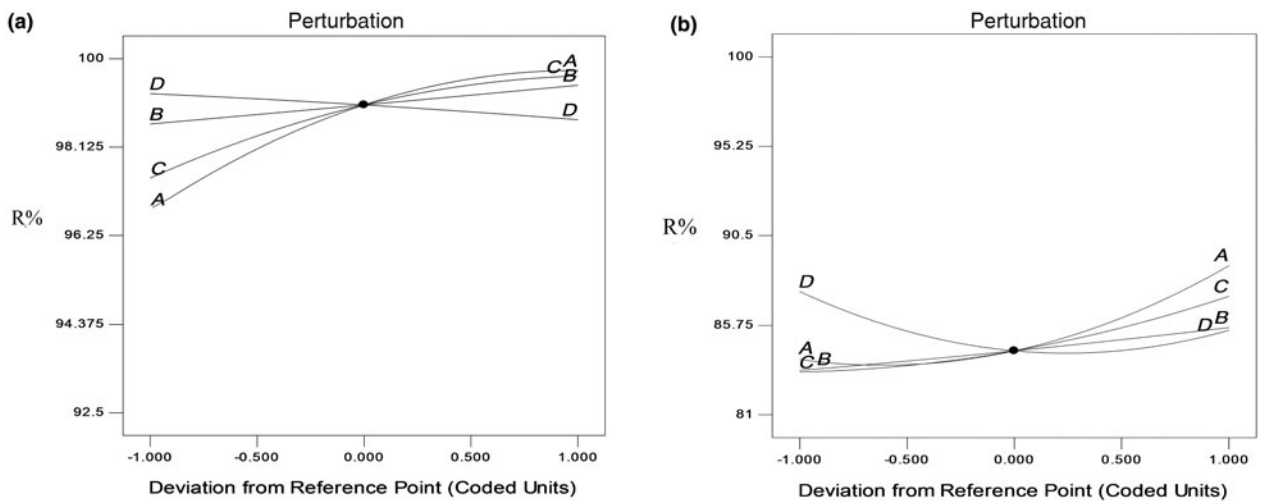


**Fig. 9.** The effect of pH (*A*), temperature (*B*), concentration of adsorbent (*C*) and CV concentration (*D*) on dye removal (R%) by (a) Mnt-BTAC and (b) Mnt-BTAC-SDS.
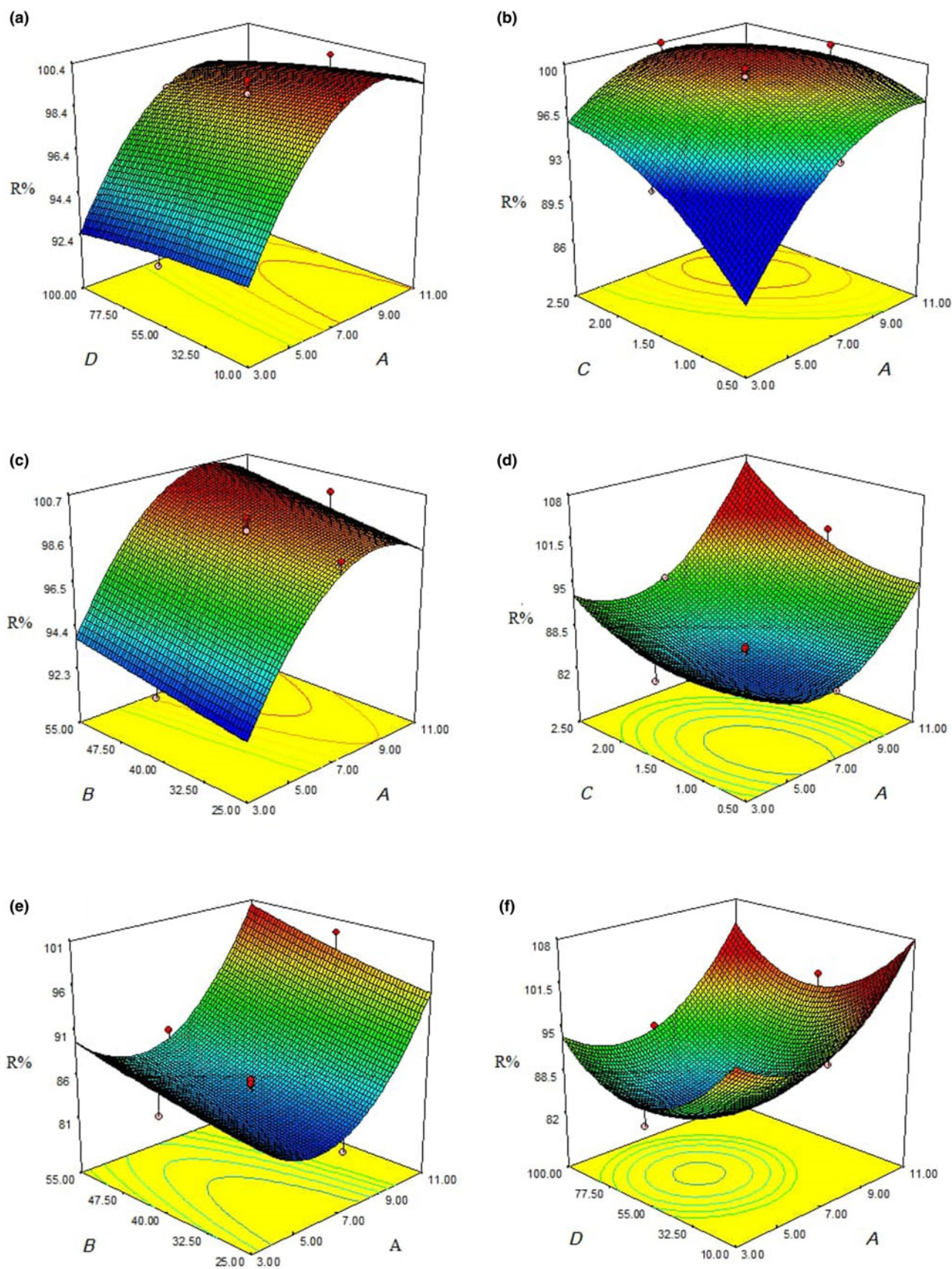
**Fig. 10.** Response surface and counter plots for Mnt-BTAC (a,b,c) and Mnt-BTAC-SDS (d,e,f): pH (*A*), temperature (*B*), concentration of adsorbent (*C*), CV concentration (*D*) and dye removal efficiency (R%).
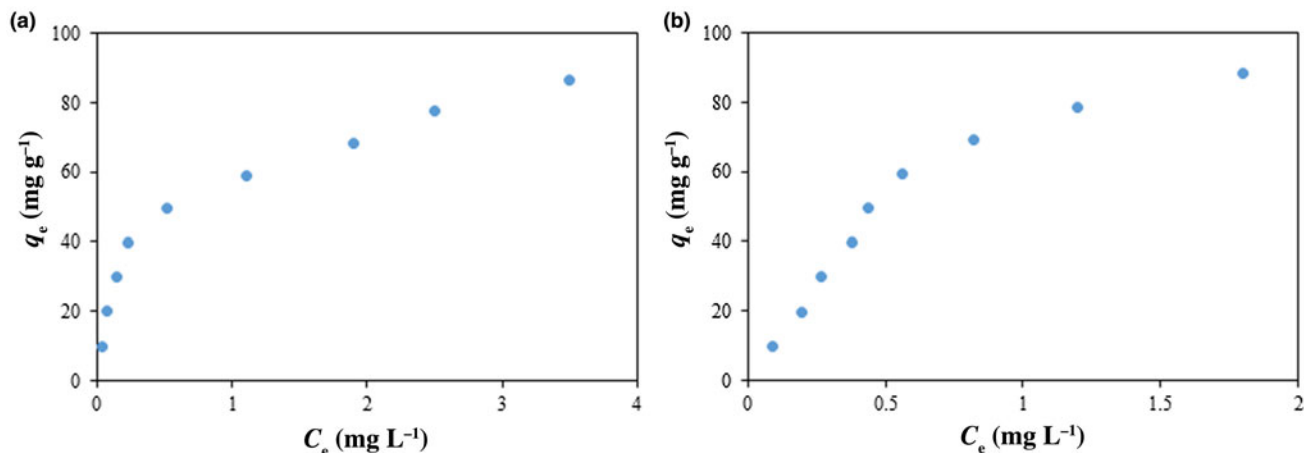
**Fig. 11.** The CV adsorption isotherm on (a) Mnt-BTAC and (b) Mnt-BTAC-SDS at optimum conditions.

Mnt-BTAC concentration. The equilibrium experiments for CV adsorption on Mnt-BTAC-SDS were performed at the optimal conditions for the solutions with concentrations of 10–100 mg L$^{-1}$. Figure 11 shows the CV adsorption isotherms for Mnt-BTAC and Mnt-BTAC-SDS.

Non-linear fitting of isotherms was performed using Flory–Huggins (Febrianto *et al.*, 2009), Langmuir (Langmuir, 1916), Redlich–Peterson (Febrianto *et al.*, 2009), Freundlich (Freundlich, 1907), Sips (Sips, 1948) and Temkin (Temkin & Pyzhev, 1940) isotherms. The equations for the adsorption isotherms are shown in Equations 4–9:

$$\text{Flory–Huggins } q_e = \frac{C_e(q_{max} - q_e)^n}{K_{FH}} \qquad (4)$$

$$\text{Langmuir } q_e = \frac{K_L q_{max} C_e}{1 + K_L C_e} \qquad (5)$$

$$\text{Redlich–Peterson } q_e = \frac{A C_e}{1 + B C_e^g} \qquad (6)$$

$$\text{Freundlich } q_e = K_F C_e^{\frac{1}{n}} \qquad (7)$$

$$\text{Sips } q_e = q_{max} \frac{(K_{LF} C_e)^{\frac{1}{n}}}{1 + (K_{LF} C_e)^{\frac{1}{n}}} \qquad (8)$$

$$\text{Temkin } q_e = B_1 \ln(A_1 C_e) \qquad (9)$$

The Langmuir isotherm assumes a homogeneous surface for the adsorbent and the Sips and Freundlich isotherms are used for heterogeneous surfaces. In these isotherms, $q_e$ (mg g$^{-1}$) is the adsorbed CV on the surface, $C_e$ (mg L$^{-1}$) is the CV equilibrium concentration, $q_{max}$ (mg g$^{-1}$) is the maximum adsorption capacity, n is an empirical constant related to surface heterogeneity and $K_L$, $K_F$, $K_{LF}$ and $K_{FH}$ are the Langmuir, Freundlich, Sips and Flory–Huggins constants. $B_1$ is a constant related to the heat of adsorption. $A_1$ is the Temkin equilibrium isotherm constant. The Redlich–Peterson model assumes both monolayer and multilayer adsorption and g, A and B are the Redlich–Peterson constants.

The equilibrium data for CV adsorption on the two surfactant-modified Mnts have been fitted with isotherm equations (Table 6). The goodness of fit of the equilibrium data to the isotherms for both Mnt-BTAC and Mnt-BTAC-SDS is according to the following order: Temkin > Sips > Redlich–Peterson. For both surfactant-modified Mnt components, the Temkin isotherms assumes that the heat of adsorption decreases linearly with loading due to adsorbate–adsorbent interactions (Foo & Hameed, 2010). The maximum adsorption capacities of Mnt-BTAC and Mnt-BTAC-SDS for CV (267.16 and 321.48 mg g$^{-1}$, respectively) were obtained using the Sips isotherm at 25°C. Therefore, Mnt-BTAC-SDS has a greater adsorption capacity for CV compared to Mnt-BTAC.

**Table 6.** The fitting parameters of the adsorption isotherms for CV adsorption on Mnt-BTAC and Mnt-BTAC-SDS.

| Models | Parameters | Mnt-BTAC | Mnt-BTAC-SDS |
|---|---|---|---|
| Langmuir | $q_{max}$ (mg g$^{-1}$) | 157.70 | 297.68 |
| | $K_L$ (L mg$^{-1}$) | 0.536 | 0.359 |
| | $R^2$ | 0.9602 | 0.9289 |
| Freundlich | $K_F$ (L mg$^{-1}$) | 56.83 | 67.64 |
| | n | 2.55 | 1.80 |
| | $R^2$ | 0.9805 | 0.9308 |
| Redlich–Peterson | A (L g$^{-1}$) | 6078 | 6000 |
| | B (L mg$^{-1}$) | 105.88 | 90.28 |
| | g (L mg$^{-1}$) | 0.6716 | 0.4835 |
| | $R^2$ | 0.9823 | 0.98361 |
| Temkin | $B_1$ (mg g$^{-1}$) | 15.34 | 9.30 |
| | $A_1$ (L mg$^{-1}$) | 48.86 | 32.39 |
| | $R^2$ | 0.9836 | 0.9885 |
| Sips | $q_{max}$ (mg g$^{-1}$) | 267.16 | 321.48 |
| | $K_{LF}$ (L mg$^{-1}$) | 0.054 | 0.128 |
| | n | 2.22 | 1.54 |
| | $R^2$ | 0.9827 | 0.9500 |
| Flory–Huggins | $q_{max}$ (mg g$^{-1}$) | 250.99 | 329.99 |
| | $K_{FH}$ | 89.99 | 80.00 |
| | n | 1.8 | 1.5 |
| | $R^2$ | 0.9584 | 0.9306 |

### Kinetic models

Kinetic studies of CV adsorption on the two surfactant-modified Mnts were carried out at optimum conditions. The results are shown in Fig. 12.
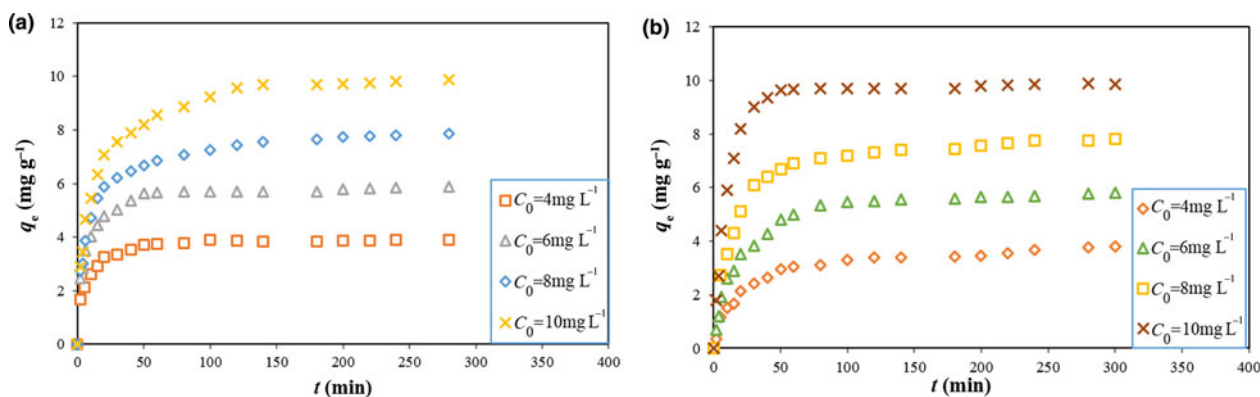
**Fig. 12.** Kinetic adsorption data of CV dye on (a) Mnt-BTAC and (b) Mnt-BTAC-SDS at optimum conditions.

The pseudo-first order (PFO) (Lagergren, 1898), pseudo-second order (PSO) (Ho, 2006), Elovich (Zeldowitsch, 1934), modified pseudo-first order (MPFO) (Yang & Al-Duri, 2005; Azizian & Bashiri, 2008), intraparticle diffusion (ID) (Weber & Morris, 1963), integrated kinetics Langmuir (IKL) (Marczewski, 2010) and fractal-like integrated kinetics Langmuir (FL-IKL) (Haerifar & Azizian, 2012) kinetic models were tested in this study. Most similar studies in the past have used linear fitting for the kinetic models. However, it has been shown recently that application of linear fitting to kinetic models might be erroneous (Simonin, 2016), so we applied non-linear fitting for our kinetic study, as shown in Equations 10–16:

$$\text{PFO model} \quad \frac{q}{q_e} = 1 - \exp(-k_1 t) \qquad (10)$$

$$\text{PSO model} \quad \frac{q}{q_e} = \frac{k_2^* t}{1 + k_2^* t} \quad (k_2^* = k_2 q_e) \qquad (11)$$

$$\text{Elovich model} \quad \frac{q}{q_e} = \frac{1}{\beta q_e} \ln(\alpha\beta) + \frac{1}{\beta q_e} \ln t \qquad (12)$$

$$\text{MPFO model} \quad \frac{q}{q_e} = \ln q_e - k_m t + \ln(q_e - q) \qquad (13)$$

$$\text{ID model} \quad q_t = k_i t^{\frac{1}{2}} + I \qquad (14)$$

$$\text{IKL model} \quad \frac{q}{q_e} = \frac{(1 - e^{-k_L t})}{(1 - a e^{-k_L t})} \qquad (15)$$

$$\text{FL} - \text{IKL model} \quad \frac{q}{q_e} = \frac{(1 - e^{-k_{FL} t^n})}{(1 - f e^{-k_{FL} t^n})} \qquad (16)$$

where $q$ is the amount of adsorbed CV onto surfactant-modified Mnt components and $k_1$, $k_2$, $k_m$, $k_i$, $k_L$ and $k_{FL}$ are the rate

**Table 7.** Kinetic parameters of CV adsorption on Mnt-BTAC.

| Models | Parameters | $C_0$ (mg L$^{-1}$) | | | |
|---|---|---|---|---|---|
| | | 4 | 6 | 8 | 10 |
| PFO | $k_1$ (1 min$^{-1}$) | 0.1201 | 0.1317 | 0.0854 | 0.0703 |
| | $R^2$ | 0.9229 | 0.9185 | 0.8801 | 0.9020 |
| PSO | $k_2$ (mg (g min$^{-1}$)$^{-1}$) | 0.0654 | 0.0430 | 0.0196 | 0.0134 |
| | $R^2$ | 0.9858 | 0.9892 | 0.9850 | 0.9877 |
| Elovich | $\alpha$ (mg (g min$^{-1}$)$^{-1}$) | 17.664 | 22.678 | 8.132 | 6.1073 |
| | $\beta$ (g mg$^{-1}$) | 2.227 | 1.455 | 0.9253 | 0.6715 |
| | $R^2$ | 0.9024 | 0.9080 | 0.9667 | 0.9729 |
| MPFO | $k_m$ (1 min$^{-1}$) | 0.0255 | 0.0211 | 0.0161 | 0.0180 |
| | $R^2$ | 0.7751 | 0.7985 | 0.9757 | 0.9694 |
| ID | $k_i$ | 0.1695 | 0.274 | 0.4057 | 0.5467 |
| | $I$ | 1.877 | 2.7096 | 2.910 | 3.2510 |
| | $R^2$ | 0.6270 | 0.6486 | 0.7624 | 0.8019 |
| IKL | $k_L$ (1 min$^{-1}$) | 0.00015 | 0.00015 | 0.00011 | 0.00010 |
| | $a$ | 0.9993 | 0.9993 | 0.9992 | 0.9992 |
| | $R^2$ | 0.9841 | 0.9882 | 0.9844 | 0.9875 |
| FL-IKL | $f$ | 0.9992 | 0.9993 | 0.9992 | 0.9992 |
| | $n$ | 1.0997 | 1.0279 | 0.9156 | 0.9626 |
| | $k_{FL}$ (1 min$^{-1}$) | 0.00012 | 0.00015 | 0.00013 | 0.00010 |
| | $R^2$ | 0.9768 | 0.9864 | 0.9905 | 0.9891 |

**Table 8.** Kinetic parameters of CV adsorption on Mnt-BTAC-SDS.

| Models | Parameters | $C_0$ (mg L$^{-1}$) | | | |
|---|---|---|---|---|---|
| | | 4 | 6 | 8 | 10 |
| PFO | $k_1$ (1 min$^{-1}$) | 0.033 | 0.042 | 0.051 | 0.088 |
| | $R^2$ | 0.9318 | 0.9714 | 0.9613 | 0.9975 |
| PSO | $k_2$ (mg (g min$^{-1}$)$^{-1}$) | 0.0163 | 0.0135 | 0.0128 | 0.0167 |
| | $R^2$ | 0.9818 | 0.9897 | 0.9905 | 0.9672 |
| Elovich | $\alpha$ (mg (g min$^{-1}$)$^{-1}$) | 0.7076 | 0.1237 | 3.3975 | 5.9385 |
| | $\beta$ (g mg$^{-1}$) | 1.4704 | 0.8939 | 0.8040 | 0.6279 |
| | $R^2$ | 0.9786 | 0.9712 | 0.9248 | 0.8441 |
| MPFO | $k_m$ (1 min$^{-1}$) | 0.0098 | 0.0135 | 0.0147 | 0.0261 |
| | $R^2$ | 0.9360 | 0.9373 | 0.9449 | 0.8419 |
| ID | $k_i$ | 0.1933 | 0.3257 | 0.3677 | 0.4844 |
| | $I$ | 0.9370 | 1.4319 | 2.8478 | 3.8580 |
| | $R^2$ | 0.8345 | 0.8134 | 0.7398 | 0.6179 |
| IKL | $k_L$ (1 min$^{-1}$) | 0.00004 | 0.00006 | 0.0077 | 0.00011 |
| | $a$ | 0.9992 | 0.9992 | 0.9126 | 0.9993 |
| | $R^2$ | 0.9916 | 0.9898 | 0.9953 | 0.9674 |
| FL-IKL | $f$ | 0.9992 | 0.9992 | 0.9992 | 0.9991 |
| | $n$ | 1.0468 | 1.1563 | 1.2518 | 1.5769 |
| | $k_{FL}$ (1/min$^\alpha$) | 0.00004 | 0.00003 | 0.00003 | 0.00003 |
| | $R^2$ | 0.9907 | 0.9933 | 0.9908 | 0.9955 |
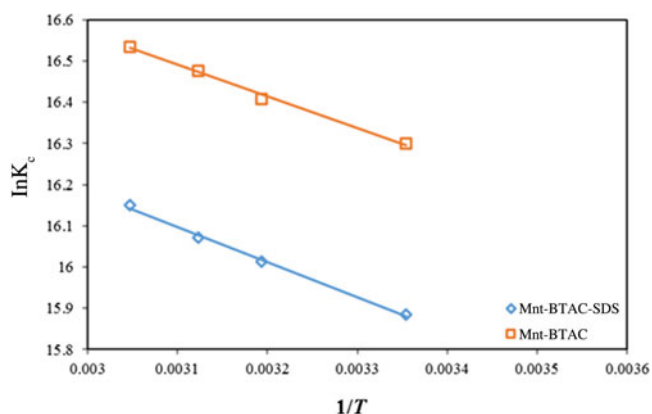
**Fig. 13.** The plot of $\ln K_c$ *vs* $1/T$ for Mnt-BTAC and Mnt-BTAC-SDS.

constants for the PFO, PSO, MPFO, ID, IKL, and FL-IKL kinetic models, respectively, *t* is the adsorption time and I is a constant parameter. In the Elovich kinetic model, α is the adsorption rate at the beginning of adsorption and β is constant related to the extent of surface coverage and activation energy for chemisorption. In the IKL and FL-IKL equations, a, n and f are constants.

The kinetic parameters and coefficients of determination for CV adsorption on the two surfactant-modified Mnts are listed in Tables 7 & 8. The IKL and FL-IKL kinetic models fit the kinetics data more accurately. In addition, the comparison of the $R^2$ values of the various kinetic models for both modified Mnt components indicates that the FL-IKL model ($R^2 > 0.99$) is the most suitable. Therefore, the adsorbents have heterogeneous and porous surfaces (Bashiri & Javanmardi, 2021).

### Thermodynamic studies

Equations 17 and 18 were used to calculate the thermodynamic parameters of CV adsorption:

$$\Delta G^{\circ} = -RT \ln K_c \qquad (17)$$

$$\ln K_c = -\frac{\Delta G^{\circ}}{RT} = \frac{\Delta S^{\circ}}{R} - \frac{\Delta H^{\circ}}{RT} \qquad (18)$$

where R is the universal gas constant, *T* is absolute temperature and $K_c$ is a dimensionless equilibrium constant calculated from the Langmuir constant (Tran *et al.*, 2016). The thermodynamic parameters of Mnt modified with BTAC and SDS were determined from the slopes of the straight lines in Fig. 13 and are listed

**Table 9.** Thermodynamic data of CV removal by Mnt-BTAC and Mnt-BTAC-SDS.

| Adsorbents | Temperature (°C) | $\Delta G^{\circ}$ (kJ mol$^{-1}$) | $\Delta H^{\circ}$ (kJ mol$^{-1}$) | $\Delta S^{\circ}$ (kJ mol$^{-1}$ K$^{-1}$) |
|---|---|---|---|---|
| Mnt-BTAC | 25 | −40.220 | | |
| | 40 | −42.597 | +6.538 | +0.156 |
| | 47 | −43.672 | | |
| | 55 | −44.951 | | |
| Mnt-BTAC-SDS | 25 | −39.369 | | |
| | 40 | −41.706 | +7.088 | +0.155 |
| | 47 | −42.797 | | |
| | 55 | −44.044 | | |

**Table 10.** Maximum CV adsorption capacities of various adsorbents.

| Adsorbent | Maximum adsorption capacity (mg g$^{-1}$) | References |
|---|---|---|
| Almond shell | 114.00 | Ishaq *et al.* (2016) |
| ZnO–nanorods–activated carbon | 113.64 | Alipanahpour Dila *et al.* (2016) |
| Soil–Ag nanoparticles | 1.92 | Satapathy & Das (2014) |
| Phosphoric acid-activated carbon | 60.42 | Senthilkumaar *et al.* (2006) |
| Zeolite from bottom ash | 17.60 | Bertolini *et al.* (2013) |
| Zeolite–Mnt | 150.52 | Sarabadan *et al.* (2019a) |
| Sulfuric acid-activated carbon | 85.84 | Senthilkumaar *et al.* (2006) |
| Zeolite from fly ash | 19.60 | Bertolini *et al.* (2013) |
| Natural zeolite | 177.75 | Sarabadan *et al.* (2019b) |
| Kaolin | 47.27 | Nandi *et al.* (2008) |
| Amino silica | 40.00 | Yang *et al.* (2014) |
| Grapefruit peel | 254.16 | Yagub *et al.* (2014) |
| Wheat bran | 80.37 | Yagub *et al.* (2014) |
| Japonica | 82.83 | Yagub *et al.* (2014) |
| Pineapple leaf powder | 78.22 | Yagub *et al.* (2014) |
| Sawdust | 37.83 | Yagub *et al.* (2014) |
| Rice husk | 44.87 | Yagub *et al.* (2014) |
| Mnt–hyamine | 299.99 | Sarabadan *et al.* (2021) |
| Magnetic zeolite | 0.9711 | Amodu *et al.* (2015) |
| Merck activated carbon | 84.11 | Sarabadan *et al.* (2019a) |
| Mnt nanoparticles | 616.07 | Sarabadan *et al.* (2021) |
| Mnt-BTAC | 267.16 | This work |
| Mnt-BTAC-SDS | 321.48 | This work |

in Table 9. The low and positive values of Δ*H*° for CV adsorption on the surfactant-modified Mnts indicate physical and endothermic adsorption. This is in accordance with increased CV adsorption at greater temperatures. The positive Δ*S*° values for the surfactant-modified Mnts confirmed the increased disorder in solution during adsorption. The Δ*G*° values for the surfactant-modified Mnts are negative, reflecting the spontaneity of the adsorption processes.

### Comparison with other adsorbents

Table 10 shows the maximum adsorption capacity of CV by Mnt nanoparticles, the surfactant-modified Mnts (this work) and other adsorbents reported in the literature (Senthilkumaar *et al.*, 2006; Nandi *et al.*, 2008; Bertolini *et al.*, 2013; Satapathy & Das, 2014; Yang *et al.*, 2014; Amodu *et al.*, 2015; Alipanahpour Dila *et al.*, 2016; Ishaq *et al.*, 2016; Sarabadan *et al.*, 2021). The maximum adsorption capacity of Mnt-BTAC-SDS is greater than those of some synthesized adsorbents that are expensive or difficult to prepare. The maximum adsorption capacity of Mnt nanoparticles for CV (616.07 mg g$^{-1}$) is greater than those of Mnt-BTAC (267.16 mg g$^{-1}$) and Mnt-BTAC-SDS (321.48 mg g$^{-1}$). Although Mnt nanoparticles have a large adsorption capacity, their separation from solution is difficult and requires ultra-high-speed centrifugation. Therefore, Mnt-BTAC-SDS could represent an affordable adsorbent for CV removal from aqueous solutions.

### Summary and conclusions

This study aimed to modify Mnt nanoparticles first with BTAC surfactant and then with BTAC and SDS surfactants. The

variables that control CV removal by the surfactant-modified adsorbents were optimized. The structure and morphology of the surfactant-modified Mnts were studied using FTIR, XRD, BET, FE-SEM and EDX analysis. RSM was used to indicate the importance of the variables pH, temperature, concentration of adsorbent and CV concentration in terms of dye removal. For Mnt-BTAC, CV adsorption was optimized at pH 9, temperature 25°C, concentration of adsorbent 1 g L$^{-1}$ and CV concentration 50 mg L$^{-1}$. For Mnt-BTAC-SDS, CV adsorption was optimized at pH 10.1, temperature 33.29°C, concentration of adsorbent 0.98 g L$^{-1}$ and CV concentration 10.44 mg L$^{-1}$. pH is the variable that has the greatest impact on CV adsorption. pH, temperature and concentration of adsorbent have positive impacts on CV removal and CV concentration has a negative impact on CV removal. The equilibrium and kinetic data of CV adsorption onto Mnt-BTAC and Mnt-BTAC-SDS best fit the Temkin and FL-IKL models. CV adsorption on these two surfactant-modified Mnts was endothermic and physisorption. The maximum adsorption capacities of the modified Mnts were compared with those of other adsorbents. Mnt-BTAC-SDS could represent a suitable CV adsorbent and might be beneficial in wastewater purification.

## References

Acisli O., Khataee A., Karaca S. & Sheydaei M. (2016) Modification of nanosized natural montmorillonite for ultrasound-enhanced adsorption of acid red 17. *Ultrasonics Sonochemistry*, **31**, 116–121.

Agarwal S., Tyagi I., Gupta V. K., Dastkhoon M., Ghaedi M., Yousefi F. & Asfaram A. (2016) Ultrasound-assisted adsorption of sunset yellow CFC dye onto Cu doped ZnS nanoparticles loaded on activated carbon using response surface methodology based on central composite design. *Journal of Molecular Liquids*, **219**, 332–340.

Ali I., Asim M. & Khan T.A. (2012) Low cost adsorbents for the removal of organic pollutants from wastewater. *Journal of Environmental Management*, **113**, 170–183.

Alipanahpour Dila E., Ghaedi M., Ghaedi A., Asfaram A., Jamshidi M. & Purkait M.K. (2016) Application of artificial neural network and response surface methodology for the removal of crystal violet by zinc oxide nanorods loaded on activate carbon: kinetics and equilibrium study. *Journal of the Taiwan Institute of Chemical Engineers*, **59**, 210–220.

Amodu O.S., Ojumu T.V., Ntwampe S.K. & Ayanda O.S. (2015) Rapid adsorption of crystal violet onto magnetic zeolite synthesized from fly ash and magnetite nanoparticles. *Journal of Encapsulation and Adsorption Sciences*, **5**, 191–203.

Andrades M.S., Rodríguez-Cruz M.S., Sánchez-Martín M.J. & Sánchez-Camazano M. (2004) Effect of the modification of natural clay minerals with hexadecylpyridinium cation on the adsorption–desorption of fungicides. *International Journal of Environmental Analytical Chemistry*, **84**, 133–141.

Azizian S. & Bashiri H. (2008) Adsorption kinetics at the solid/solution interface: statistical rate theory at initial times of adsorption and close to equilibrium. *Langmuir*, **24**, 11669–11676.

Bashiri H. & Javanmardi A.H. (2021) Investigation of fractal-like characteristics according to new kinetic equation of desorption. *Langmuir*, **37**, 2123–2128.

Bashiri H. & Nesari S. (2019) Removal of alizarin yellow from water by activated carbon prepared from microwave radiation of rice husk: thermodynamic, equilibrium and kinetic study. *Journal of Applied Chemistry* **14**, 335–352.

Bertolini T.C.R., Izidoro J.C., Magdalena C.P. & Fungaro D.A. (2013) Adsorption of crystal violet dye from aqueous solution onto zeolites from coal fly and bottom ashes. *Orbital: The Electronic Journal of Chemistry*, **5**, 179–191.

Carrizosa M.J., Koskinen W.C., Hermosin M.C. & Cornejo J. (2001) Dicamba adsorption–desorption on organoclays. *Applied Clay Science*, **18**, 223–231.

Chen L., Zhou C.H., Fiore S., Tong D.S., Zhang H., Li C.S., Ji S.F. & Yu W.H. (2016) Functional magnetic nanoparticle/clay mineral nanocomposites: preparation, magnetism and versatile applications. *Applied Clay Science*, **127–128**, 143–163.

Eris S. & Bashiri H. (2016) Kinetic study of the adsorption of dyes onto activated carbon. *Progress in Reaction Kinetics and Mechanism*, **41**, 109–119.

Falaki Z. & Bashiri H. (2021) Preparing an adsorbent from the unused solid waste of rosewater extraction for high efficient removal of crystal violet. *Journal of the Iranian Chemical Society*, **18**, 2689–2702.

Febrianto J., Kosasih A.N., Sunarso J., Ju Y.-H., Indraswati N. & Ismadji S. (2009) Equilibrium and kinetic studies in adsorption of heavy metals using biosorbent: a summary of recent studies. *Journal of Hazardous Materials*, **162**, 616–645.

Foo K.Y. & Hameed B.H. (2010) Insights into the modeling of adsorption isotherm systems. *Chemical Engineering Journal*, **156**, 2–10.

Freundlich H. (1907) Über die Adsorption in Lösungen. *Zeitschrift für Physikalische Chemie*, 57U, 385.

Haerifar M. & Azizian S. (2012) Fractal-like adsorption kinetics at the solid/solution interface. *Journal of Physical Chemistry C*, **116**, 13111–13119.

Ho Y.-S. (2006) Review of second-order models for adsorption systems. *Journal of Hazardous Materials*, **136**, 681–689.

Ishaq M., Javed F., Amad I., Ullah H., Hadi F. & Sultan S. (2016) Adsorption of crystal violet dye from aqueous solutions onto low-cost untreated and NaOH treated almond shell. *Iranian Journal of Chemistry and Chemical Engineering (IJCCE)*, **35**, 97–106.

Kıranşan M., Soltani R.D.C., Hassani A., Karaca S. & Khataee A. (2014) Preparation of cetyltrimethylammonium bromide modified montmorillonite nanomaterial for adsorption of a textile dye. *Journal of the Taiwan Institute of Chemical Engineers*, **45**, 2565–2577.

Koh S.-M. & Dixon J.B. (2001) Preparation and application of organominerals as sorbents of phenol, benzene and toluene. *Applied Clay Science*, **18**, 111–122.

Lagergren S. (1898) Zur theorie der sogenannten adsorption geloster stoffe. *Kungliga Svenska Vetenskapsakademiens. Handlingar*, **24**, 1–39.

Langmuir I. (1916) The constitution and fundamental properties of solids and liquids. Part I. Solids. *Journal of the American Chemical Society*, **38**, 2221–2295.

Li S. (2010) Removal of crystal violet from aqueous solution by sorption into semi-interpenetrated networks hydrogels constituted of poly(acrylic acid-acrylamide-methacrylate) and amylose. *Bioresource Technology*, **101**, 2197–2202.

Liu B., Wang X., Yang B. & Sun R. (2011) Rapid modification of montmorillonite with novel cationic Gemini surfactants and its adsorption for methyl orange. *Materials Chemistry and Physics*, **130**, 1220–1226.

Marczewski A.W. (2010) Analysis of kinetic Langmuir model. Part I: integrated kinetic Langmuir equation (IKL): a new complete analytical solution of the Langmuir rate equation. *Langmuir*, **26**, 15229–15238.

Mousavi S.M. & Nakhostin Panahi P. (2016) Modeling and optimization of NH$_3$-SCR performance of MnO$_x$/γ-alumina nanocatalysts by response surface methodology. *Journal of the Taiwan Institute of Chemical Engineers*, **69**, 68–77.

Mousavi S.M., Salari D., Niaei A., Panahi P.N. & Shafiei S. (2014) A modelling study and optimization of catalytic reduction of NO over CeO$_2$–MnO$_x$ (0.25)–Ba mixed oxide catalyst using design of experiments. *Environmental Technology*, **35**, 581–589.

Nandi B.K., Goswami A., Das A.K., Mondal B. & Purkait M.K. (2008) Kinetic and equilibrium studies on the adsorption of crystal violet dye using kaolin as an adsorbent. *Separation Science and Technology*, **43**, 1382–1403.

Park Y., Ayoko G.A., Kurdi R., Horváth E., Kristóf J. & Frost R.L. (2013) Adsorption of phenolic compounds by organoclays: implications for the removal of organic pollutants from aqueous media. *Journal of Colloid and Interface Science*, **406**, 196–208.

Santhana Krishna Kumar A., Ramachandran R., Kalidhasan S., Rajesh V. & Rajesh N. (2012) Potential application of dodecylamine modified sodium montmorillonite as an effective adsorbent for hexavalent chromium. *Chemical Engineering Journal*, **211–212**, 396–405.

Sarabadan M., Bashiri H. & Mousavi S.M. (2019a) Adsorption of crystal violet dye by zeolite–montmorillonite: modeling, kinetic and equilibrium studies. *Clay Minerals*, **54**, 357–368.

Sarabadan M., Bashiri H. & Mousavi S.M. (2019b) Removal of crystal violet dye by an efficient and low cost adsorbent: modeling, kinetic, equilibrium and thermodynamic studies. *Korean Journal of Chemical Engineering*, **36**, 1575–1586.

Sarabadan M., Bashiri H. & Mousavi S.M. (2021) Modelling, kinetics and equilibrium studies of crystal violet adsorption on modified montmorillonite by sodium dodecyl sulfate and hyamine surfactants. *Clay Minerals*, **56**, 16–27.

Sarma G.K., Sen Gupta S. & Bhattacharyya K.G. (2016) Adsorption of crystal violet on raw and acid-treated montmorillonite, K10, in aqueous suspension. *Journal of Environmental Management*, **171**, 1–10.

Satapathy M.K. & Das P. (2014) Optimization of crystal violet dye removal using novel soil-silver nanocomposite as nanoadsorbent using response surface methodology. *Journal of Environmental Chemical Engineering*, **2**, 708–714.

Senthilkumaar S., Kalaamani P. & Subburaam C.V. (2006) Liquid phase adsorption of crystal violet onto activated carbons derived from male flowers of coconut tree. *Journal of Hazardous Materials*, **136**, 800–808.

Shirzad-Siboni M., Khataee A., Hassani A. & Karaca S. (2015) Preparation, characterization and application of a CTAB-modified nanoclay for the adsorption of an herbicide from aqueous solutions: kinetic and equilibrium studies. *Comptes Rendus Chimie*, **18**, 204–214.

Simonin J.-P. (2016) On the comparison of pseudo-first order and pseudo-second order rate laws in the modeling of adsorption kinetics. *Chemical Engineering Journal*, **300**, 254–263.

Sips R. (1948) On the structure of a catalyst surface. *Journal of Chemical Physics*, **16**, 490–495.

Temkin M.J. & Pyzhev V. (1940) Recent modification to Langmiur isotherms. *Acta Physicochimica URSS*, **12**, 327–356.

Tran H.N., You S.-J. & Chao H.-P. (2016) Thermodynamic parameters of cadmium adsorption onto orange peel calculated from various methods: a comparison study. *Journal of Environmental Chemical Engineering*, **4**, 2671–2682.

Warr, L.N. (2020) Recommended abbreviations for the names of clay minerals and associated phases. *Clay Minerals*, **55**, 261–264.

Weber W.J. & Morris J.C. (1963) Kinetics of adsorption on carbon from solution. *Journal of the Sanitary Engineering Division*, **89**, 31–60.

Yagub M.T., Sen T.K., Afroze S. & Ang H.M. (2014) Dye and its removal from aqueous solution by adsorption: a review. *Advances in Colloid and Interface Science*, **209**, 172–184.

Yang H., Zhou D., Chang Z. & Zhang L. (2014) Adsorption of crystal violet onto amino silica: optimization, equilibrium, and kinetic studies. *Desalination and Water Treatment*, **52**, 6113–6121.

Yang X. & Al-Duri B. (2005) Kinetic modeling of liquid-phase adsorption of reactive dyes on activated carbon. *Journal of Colloid and Interface Science*, **287**, 25–34.

Zeldowitsch J. (1934) Über den mechanismer der katalytischen oxydation von CO an $MnO_2$. *Acta Physicochimica URSS*, **1**, 449–464.

Zhu R., Chen Q., Liu H., Ge F., Zhu L., Zhu J. & He H. (2014) Montmorillonite as a multifunctional adsorbent can simultaneously remove crystal violet, cetyltrimethylammonium, and 2-naphthol from water. *Applied Clay Science*, **88–89**, 33–38.